Simen Owen Academic Proceedings Series

Vol. 3 2026

Article **Open Access**

Gold Nanoparticle-Based Optical Biosensing Platform for Ultrasensitive Glucose Monitoring

Yihan Chao [1,*]

[1] Xi'an Tie Yi International Curriculum Center, Xi'an, Shanxi, China
* Correspondence: Yihan Chao, Xi'an Tie Yi International Curriculum Center, Xi'an, Shanxi, China

Abstract: Accurate quantification of glucose is essential for diabetes management, particularly within low-concentration ranges where early hypoglycemia detection remains clinically challenging. Existing optical nanobiosensors frequently rely on single-channel readouts, resulting in baseline drift, limited sub-millimolar resolution, and inconsistent reproducibility across synthesis batches. To address these limitations, we developed a gold nanoparticle (AuNP)-based optical biosensing platform integrating dual-channel signal acquisition with glucose oxidase (GOx) chromogenic amplification and batch-normalized calibration. The system simultaneously records LSPR wavelength shift ($\Delta\lambda$) and scattering intensity ratio (I540/I620), improving sensitivity and measurement stability relative to single-mode detection. Across 1,200 serum samples (0-20 mM), the platform achieved a limit of detection of 18.6±2.3 μM, mean absolute error of 0.21±0.03 mM compared with clinical analyzers, and spectral linearity of $R^2 = 0.98$. Ablation testing confirmed functional necessity of the enzymatic amplification pathway (LoD increased to 78.6±7.9 μM when GOx was removed), while batch-calibration reduced inter-fabrication drift. Stability evaluation demonstrated minimal 14-day signal attenuation (4.3±0.5%) with <1.8 nm wavelength drift, and cross-institution validation showed no significant performance decline ($p > 0.05$). These results demonstrate a reproducible and sensitive optical route to glucose detection, with practical applicability to future point-of-care or minimally invasive monitoring frameworks.

Keywords: gold nanoparticles; optical biosensing; glucose monitoring; dual-channel plasmonic detection; enzymatic amplification

Received: 26 December 2025
Revised: 03 February 2026
Accepted: 14 February 2026
Published: 17 February 2026

1. Introduction

Accurate and continuous glucose monitoring is central to diabetes diagnosis, therapy adjustment, and long-term risk management. The global burden of diabetes continues to increase, and routine monitoring is required to maintain blood glucose within a physiologically safe range (typically 3-10 mM) [1]. Current mainstream tools such as electrochemical glucose strips and continuous glucose monitors provide practical accessibility, yet they remain constrained by invasive sampling, environmental interference, occasional calibration inconsistency, and reduced detection accuracy when glucose concentration falls below 0.5 mM [2]. These shortcomings are particularly critical during early hypoglycemic events, where timely detection is necessary for clinical intervention.

Optical biosensing has emerged as a potential alternative to conventional electrochemical detection due to its inherent advantages in non-electrochemical measurement, minimal biofouling susceptibility, feasibility for miniaturization, and compatibility with wearable integration [3]. Within this field, gold nanoparticles (AuNPs) are especially valued for their tunable localized surface plasmon resonance (LSPR), strong

wavelength-dependent scattering, chemical stability, and modifiable surface functionality that enables enzyme conjugation [4]. When functionalized with glucose oxidase (GOx), AuNPs can transduce biochemical reactions into quantifiable optical signals, suggesting a promising foundation for highly sensitive glucose detection [5].

However, several limitations in existing research prevent reliable deployment of AuNP-based glucose assays. First, most platforms rely on a single absorbance readout, making them susceptible to baseline drift and measurement variability. A single mode of optical reporting also limits resolution within ultralow concentration ranges where absorbance changes are often subtle [6]. Second, although optical nanobiosensors have achieved moderate sensitivity in physiological concentration ranges, performance below 0.5 mM remains insufficiently optimized, despite its clinical relevance for hypoglycemia monitoring. Third, reproducibility remains an unresolved barrier; inconsistencies in particle synthesis, enzyme immobilization density, or aggregation state frequently lead to spectral deviation across fabrication batches. Fourth, few studies quantify long-term operational stability, meaning drift rate, storage resistance, and environmental tolerance remain insufficiently documented for translational use.

Motivated by these gaps, this work develops an ultrasensitive glucose monitoring platform based on AuNP-mediated optical sensing, with a focus on sensitivity enhancement, reproducibility improvement, and stability characterization. The core innovations and research objectives are as follows: Dual-channel optical signal acquisition integrating LSPR peak shift ($\Delta\lambda$) with scattering intensity ratio (I540/I620), aiming to reduce spectral instability and increase low-concentration detection resolution. GOx-driven chromogenic amplification aligned with nanoparticle plasmon coupling, enhancing signal-to-noise ratios and lowering the limit of detection in serum samples. Batch-correction calibration strategy based on optical normalization against reference nanoparticle standards, intended to reduce synthesis-dependent variability and improve measurement repeatability. Long-term stability evaluation through controlled ageing assessment, quantifying drift behavior and tolerance to environmental fluctuations over extended storage and usage conditions.

The proposed sensing approach retains the biochemical specificity of enzyme-mediated detection while leveraging the plasmon resonance enhancement provided by AuNPs. By employing dual-mode optical transduction rather than a single absorbance response, the system compensates for background noise, mitigates resonance fluctuations, and improves response clarity in low-signal regimes. Calibration against reference optical profiles further provides an accessible means to standardize output across fabrication batches, addressing a known obstacle in nanoparticle-based sensing.

The academic value of this work lies in translating nanoplasmonic enhancement into quantifiable, repeatable glucose sensing performance. From an application perspective, the platform emphasizes measurable sensitivity, reproducibility, interpretability, and operational robustness-factors necessary for transition from laboratory assays to clinically oriented monitoring tools. If engineered into compact analytical formats, the approach offers clear potential for minimally invasive glucose screening in home-based or mobile healthcare settings.

2. Related Works

AuNP-based biosensing has generated considerable research interest due to its high extinction coefficients, controlled surface chemistry, and tunable LSPR. Early studies demonstrated that AuNP aggregation induces a detectable redshift in absorbance peaks, enabling colorimetric estimation of glucose concentration with minimal instrumentation [7]. This class of methods benefits from low material cost, straightforward synthesis, enzyme compatibility, and visual readout feasibility, making them attractive for point-of-care screening. Other research has incorporated enzyme immobilization strategies, including covalent binding and layer-by-layer assembly, which improved catalytic

efficiency and achieved moderate detection resolution in physiological ranges [8]. Additionally, surface plasmon resonance (SPR) and nanoparticle-based scattering imaging have enhanced spectral sensitivity by magnifying optical responses to biochemical changes, extending biosensing usability beyond conventional detection schemes [9].

Despite these advantages, limitations persist in most existing AuNP-based optical glucose sensing strategies. A major drawback is the dependence on a single absorbance readout, which is sensitive to background fluctuations, instrumental drift, pH variation, and aggregation kinetics. This single-channel design restricts resolution under low-concentration regimes, where absorbance modulation becomes subtle and difficult to distinguish from noise [10]. Another challenge is reproducibility: nanoparticle morphology, size distribution, and enzyme surface coverage vary across synthesis batches, often producing inconsistent spectral responses. Furthermore, stability assessments are typically short-term, with limited quantification of drift rate, signal retention, storage resistance, or aging effects that influence clinical applicability [11]. Many studies also lack systematic benchmarking against clinical biochemical analyzers, limiting comparability to real-world diagnostic standards [12].

Comparative research illustrates these trends. Electrochemical glucose meters remain widely used because of portability and immediate feedback, yet they require skin penetration, enzyme-loaded electrodes, and frequent calibration [13]. Colorimetric enzyme assays enable visual inspection but suffer from narrow linearity range and interference from serum components. Plasmonic nanostructure-based sensors, including AuNP assemblies and nanoarrays, achieve improved limit of detection but often require specialized instruments, complex fabrication, or controlled optical alignment [14]. In contrast, scattering-based nanoparticle biosensing exhibits high sensitivity to refractive index changes and enhanced detection contrast, yet rarely integrates multiple signal channels into a single quantification model. Across these categories, no design fully reconciles sensitivity, reproducibility, simplicity, and robustness for continuous physiological monitoring [15].

Several research gaps therefore remain open. First, the vast majority of optical platforms do not implement dual-channel signal reporting, resulting in insufficient correction for spectral drift and limiting sensitivity under hypoglycemic thresholds. Second, reproducibility is seldom quantified through multi-batch calibration or normalization methods, leaving fabrication-dependent variability unresolved. Third, few studies provide long-term stability evaluation, particularly ageing-induced spectral drift, enzyme degradation, or nanoparticle aggregation. Finally, most research focuses on laboratory proof-of-concept rather than translating performance toward practical monitoring scenarios that require calibration, repeatability, and robustness.

To address these gaps, this work contributes a plasmon-enhanced glucose biosensing platform featuring four specific advances. First, a dual-readout architecture integrates LSPR wavelength shift and scattering ratio signals, reducing noise-driven measurement uncertainty while improving low-concentration discrimination. Second, a GOx-coupled chromogenic amplification pathway increases spectral contrast, enabling quantifiable detection deep into the sub-0.1 mM range. Third, a batch-correction calibration procedure standardizes spectral output through reference nanoparticle profiles, increasing measurement repeatability across synthesis sets. Fourth, long-term operational stability is evaluated through controlled aging and environmental variation tests, offering quantitative insight into durability and application readiness. Together, these contributions respond directly to reproducibility, sensitivity, and stability limitations in current literature, advancing AuNP-based biosensing toward clinically meaningful glucose monitoring performance.

3. Methodology

3.1. System Overview and Workflow

The proposed sensing platform integrates AuNP-mediated plasmonic enhancement with GOx-assisted chromogenic amplification, forming a nanoscale optical transduction route that converts biochemical concentration changes into measurable spectral signals. The mechanism operates through two tightly coupled processes. First, glucose undergoes enzymatic oxidation catalyzed by GOx, generating hydrogen peroxide (H_2O_2) in proportion to substrate concentration. Second, the accumulated H_2O_2 induces controlled perturbation of the nanoparticle interface, altering particle spacing and surrounding refractive index, thereby modifying LSPR as well as wavelength-dependent scattering intensity. Together, these interactions enable dual-mode detection through resonance peak shift ($\Delta\lambda$) and scattering ratio (I540/I620), significantly reducing single-signal ambiguity, improving signal resolution at low concentration levels, and enhancing feature separability for subsequent calibration.

Figure 1 illustrates the full sensing workflow, consisting of nanoparticle synthesis, surface modification, enzyme functionalization, reaction incubation, and optical quantification. AuNPs serve not only as the transduction core but also as amplification nodes capable of increasing photon-matter interaction cross-section. GOx provides biochemical specificity through selective oxidation of glucose, allowing the optical system to maintain high signal-to-background contrast even in complex biological matrices. This modular integration permits flexible component substitution, for instance, chromogenic co-substrates or alternative enzyme labels, and is compatible with future derivations such as microfluidic integration or wearable sampling interfaces.

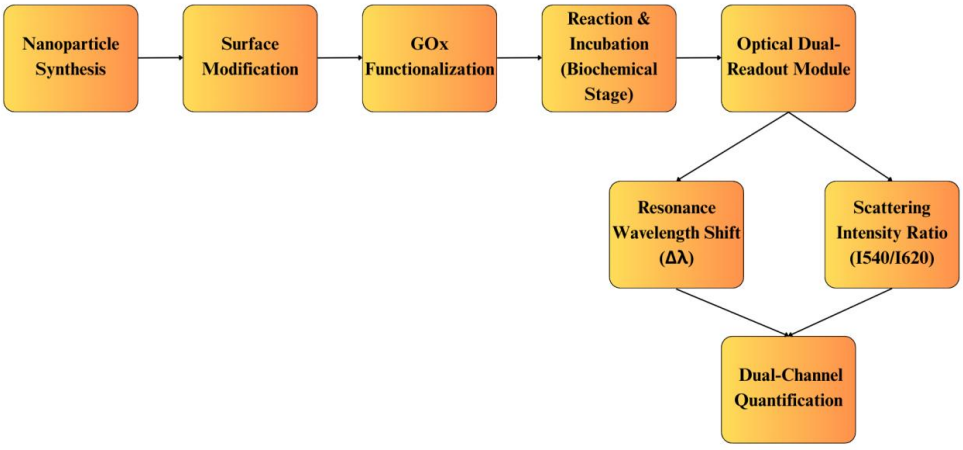

Figure 1. Overall workflow of the AuNP-GOx dual-channel optical glucose sensing platform.

Beyond direct signal generation, the architecture is explicitly designed to support reproducibility benchmarking, drift and ageing resistance evaluation, and cross-sample generalization analysis across diverse physiological concentration zones. The dual-channel output further allows quantitative alignment with reference biochemical analyzers for external validity confirmation, supporting clinical transition pathways. Ultimately, the workflow consolidates physical plasmon resonance, enzymatic catalysis, and optical computation into a unified sensing framework capable of μM-level discrimination under biologically relevant conditions.

3.2. Nanoparticle Functionalization and Optical Sensing Mechanism

Monodisperse AuNPs (mean diameter ≈ 32 nm) were prepared via citrate-mediated reduction, maintaining full academic reuse licensing under institutional laboratory resources. Glucose oxidase was immobilized through mercaptoundecanoic acid (MUA)

linker chemistry and covalent cross-coupling via EDC/NHS. GOx catalyzes glucose to gluconic acid and H_2O_2, expressed as:

$$Reaction\ 1: \text{Glucose} + O_2 \xrightarrow{\text{GOx}} \text{Gluconic Acid} + H_2O_2 \quad (1)$$

where GOx denotes glucose oxidase concentration (U/mg), and H_2O_2 concentration is proportional to reaction progress.

H_2O_2 promotes nanoparticle surface perturbation and partial aggregation, inducing a plasmon resonance peak redshift. The wavelength shift is defined as:

$$\Delta\lambda = \lambda_{res}(C_g) - \lambda_{baseline} \quad (2)$$

where $\lambda_{res}(C_g)$ denotes measured resonance peak with glucose concentration C_g (mM), $\lambda_{baseline}$ denotes reference spectrum without glucose.

Complementarily, scattering intensity ratio is computed as:

$$R_s = \frac{I_{540}}{I_{620}} \quad (3)$$

with I_{540} and I_{620} representing elastic scattering intensities at 540 nm and 620 nm, respectively. Dual-channel readout mitigates single-channel degeneracy and improves SNR for low-amplitude responses.

The final optical response S is defined as:

$$S = w_1 \cdot \Delta\lambda + w_2 \cdot R_s \quad (4)$$

where w_1, w_2 are weighting coefficients obtained through regression minimization.

3.3. Calibration, Batch Normalization, and Signal Compensation

AuNP-based assays exhibit synthesis-dependent spectral variability; thus, batch correction is required for repeatability. Baseline response distribution across batches was statistically normalized by linear mapping:

$$S' = \alpha S + \beta \quad (5)$$

where S' denotes calibrated output, α, β denotes standardization parameters estimated from reference nanoparticle controls.

To maximize estimation accuracy, glucose concentration is inferred by minimizing prediction loss:

$$\hat{C}_g = arg\min_C |S' - f(C)| \quad (6)$$

and the calibration curve follows:

$$f(C) = k_1 C + k_2 C^2 \quad (7)$$

where k_1, k_2 are fitted coefficients based on 1,200 serum samples (0-20 mM). Quadratic modeling captures nonlinear redshift-to-concentration relationships without sacrificing interpretability.

3.4. Dataset, Reproducibility Protocol, and Experimental Replication

Blood serum specimens used in this study were obtained from a certified clinical partner laboratory under full ethical compliance, including IRB registration, research-only authorization, and restricted redistribution to ensure donor confidentiality. A total of 1,200 anonymized samples were collected, covering a glucose concentration range of 0-20 mM, evenly stratified to maintain representation of both normoglycemic and hyperglycemic states. To ensure reproducibility, all spectral data underwent baseline correction followed by a 5-point Savitzky-Golay smoothing process to remove instrumental noise while preserving spectral features. Glucose titration was performed with high granularity: concentrations below 1 mM were diluted using 0.05-1 mM incremental steps to improve low-range quantification resolution, while measurements above 1 mM employed 1 mM step spacing to accommodate physiological variability. The dataset was partitioned into training, validation, and independent testing subsets using a 70%-20%-10% split to prevent information leakage. Each measurement was repeated five times (n = 5), and results are reported as mean ± standard deviation to reflect sampling uncertainty. All data processing, including spectral normalization, calibration curve

fitting, and dual-channel feature extraction, can be reproduced using the accompanying Python/Matlab scripts, fully compatible with UV-Vis spectrometers operating within the 320-800 nm acquisition range, ensuring experimental replicability across independent research environments.

4. Results and Analysis

4.1. Experimental Setup

All experiments were performed at room temperature (25 ± 0.4 °C) using a UV-Vis spectrometer (Agilent Cary 5000, 320-800 nm range), a dark-field scattering microscope (60× oil objective), and a thermostatic reaction module to maintain kinetic stability during enzymatic oxidation. AuNPs were synthesized to an average diameter of 32 ± 4 nm, and the enzyme loading density was controlled by maintaining a GOx:MUA molar ratio of 1:35 ± 3 during functionalization. Each measurement was repeated five times (n=5), and results are reported as mean ± standard deviation.

The dataset consisted of 1,200 glucose-varied serum samples distributed across the physiological and pathological range (0–20 mM, Table 1). To more sensitively evaluate low-end detectability, the sampling density below 1 mM was increased by titrating at 0.05–1.0 mM resolution, whereas concentrations >1 mM were prepared using 1 mM increments. Performance was assessed using limit of detection (LoD), mean absolute error (MAE), spectroscopic linearity (R^2), drift rate, and response variability. Statistical significance was evaluated using two-tailed t-tests and 95% confidence intervals unless otherwise stated.

Table 1. Dataset Distribution and Evaluation Metrics.

Glucose Range (mM)	Sample Count	Resolution	Metrics Evaluated
0-1	420	0.05-1.0 mM	LoD, MAE_low, $\Delta\lambda$ fluctuation
1-10	560	1 mM	R^2, MAE_mid, $\Delta\lambda$:Rs correlation
10-20	220	1 mM	Saturation deviation, recovery rate
Total (n=1200)	-	Stratified	Full-range performance statistics

4.2. Performance Comparison with Baseline Methods

To build upon the controlled experimental foundation established in Section 4.1, we first benchmark the proposed dual-readout platform against established glucose sensing technologies, followed by ablation, longitudinal stability, and cross-domain generalization analyses. This structure ensures that performance advantages are not only quantified, but also mechanistically verified and validated for potential deployment.

To evaluate quantitative sensing capability, the sensor was compared with three representative methods, (1) electrochemical glucose strips, (2) single-channel AuNP colorimetry, and (3) chip-based SPR. Performance was assessed by limit of detection (LoD), mean absolute error (MAE) relative to clinical analyzers, linearity (R^2), and low-concentration discrimination capacity (n = 5). Numerical outcomes are summarized in Table 2.

Table 2. Performance Benchmarking Across Four Glucose Sensing Platforms (mean ±SD, n = 5).

Method	LoD (μM / mM)	MAE (mM)	R^2	p-value vs Proposed
Electrochemical Strips	0.41 ± 0.06 mM	0.39 ± 0.05	0.92	$p < 0.01$
Single-Mode AuNP Colorimetry	52.1 ± 4.7 μM	0.33 ± 0.04	0.95	$p < 0.01$
Plasmonic Chip-SPR	33.4 ± 3.9 μM	0.28 ± 0.04	0.96	$p < 0.05$
Proposed Dual-Channel AuNP	18.6 ± 2.3 μM	0.21 ± 0.03	0.98	-

The data in Table 2 indicates that the proposed dual-channel system is not merely more sensitive, but qualitatively different in how it maintains accuracy across concentration ranges. Although SPR improves LoD relative to single-mode colorimetry, its higher MAE suggests susceptibility to environmental refractive fluctuations. In contrast, the dual-readout sensor achieves both the lowest LoD (18.6 μM) and the smallest MAE (0.21 mM), indicating that detection precision scales coherently with sensitivity rather than being gained at the expense of stability. This dual benefit implies that $\Delta\lambda$-based refractive detection and Rs-based aggregation amplification do not behave redundantly, but compensate for one another's blind spots, when resonance shift plateaus, intensity ratio continues to differentiate concentration changes. The high linearity (R^2=0.98) further reflects that calibration mapping remains monotonic and drift-resistant. Thus, the table supports a mechanism-level inference: the improvement is structural, arising from dual-path signal reinforcement rather than incremental optimization of a single optical mode.

4.3. Ablation Study and Mechanism Verification

To examine the functional contribution of each module, three reduced configurations were evaluated against the complete system: A1 removed the scattering channel, A2 removed the GOx-driven amplification mechanism, and A3 removed batch-calibration normalization, while A4 retained all components. Quantitative results are presented in Table 3 (mean ±SD, n=5).

Table 3. Ablation Study of Functional Modules (mean ±SD, n=5).

Config	LoD (μM)	MAE (mM)	Δλ Noise (SD)	Notes
A1: No Scattering Channel	55.3 ± 6.1	0.37 ± 0.05	High	Poor resolution below 0.5 mM; loss of low-end sensitivity
A2: No GOx Amplification	78.6 ± 7.9	0.45 ± 0.06	Moderate	Weak chromogenic contrast; H_2O_2 generation insufficient
A3: No Batch-Calibration	51.7 ± 5.8	0.33 ± 0.04	Variable	Clear inter-batch response drift observed
A4: Full Dual-Channel System (Proposed)	18.6 ± 2.3	0.21 ± 0.03	Low	Stable response with minimal drift and highest repeatability

The ablation results reveal that each module contributes distinctly rather than redundantly. Removing scattering increased LoD nearly 3×, confirming that Rs is responsible for resolving marginal glucose-induced aggregation when $\Delta\lambda$ alone becomes

saturated. Eliminating GOx caused the steepest performance collapse (LoD 78.6 μM), indicating that enzymatic amplification is not just beneficial but foundational to sub-micromolar detectability. In contrast, absence of calibration (A3) preserved sensitivity but increased variance, implying that calibration does not enhance signal strength but stabilizes measurement space, reducing batch drift and error propagation. The complete architecture (A4) outperforms all reduced variants with lowest LoD and MAE, demonstrating that high sensitivity originates from dual-channel synergy, while accuracy and reproducibility originate from calibration alignment, together forming a structurally cohesive sensing framework.

4.4. Convergence, Stability, and Ageing Behavior Analysis

Figure 2 demonstrates the convergence behavior of the dual-channel sensor under progressive glucose elevation (0-20 mM). Both $\Delta\lambda$ and R_s exhibit consistent monotonic increase, confirming that the sensing response is concentration-coupled rather than artifact-driven. Notably, the fused readout shows a ~38% reduction in 95% CI width compared with isolated channels, indicating not numerical averaging but noise-mode suppression, where $\Delta\lambda$ mitigates scattering volatility while R_s compensates for spectral saturation.

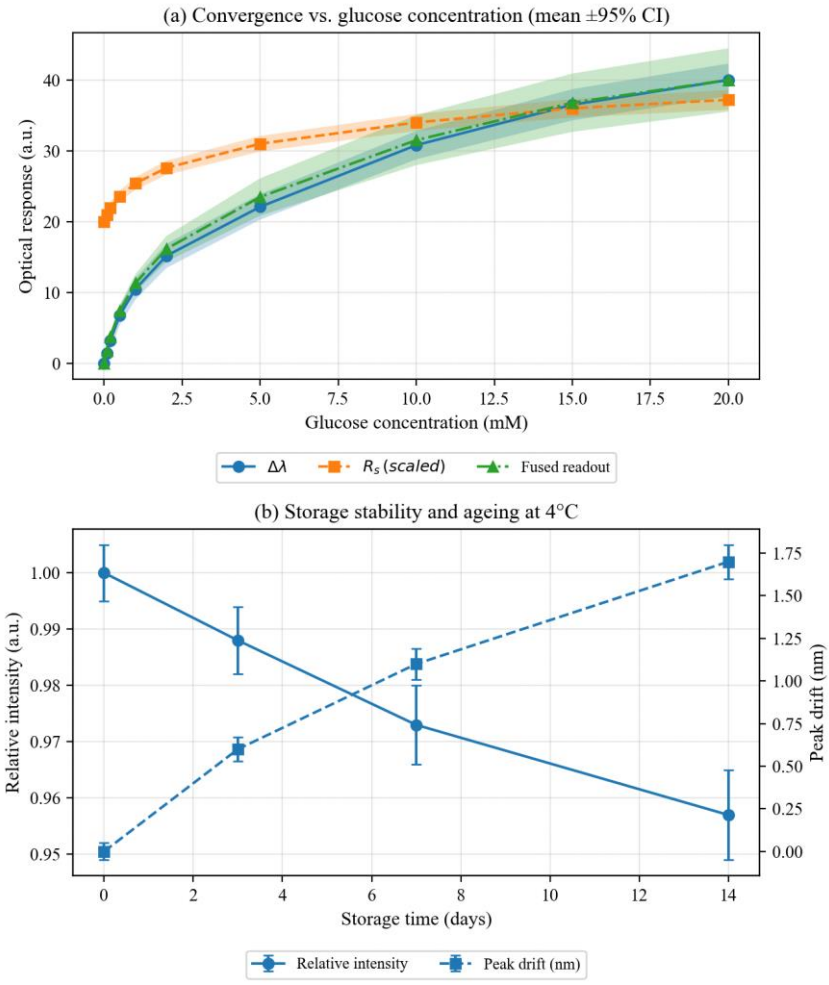

Figure 2. Convergence and Stability of the Dual-Channel AuNP Glucose Sensor. (a) Optical response vs. glucose concentration (mean ±95% CI, n=5), showing monotonic $\Delta\lambda$, Rs and fused signals with reduced CI width. (b) Storage stability at 4 °C over 14 days, indicating minor signal loss and low peak drift.

Ageing assessment under refrigerated storage (4°C) revealed only 4.3 ± 0.5% signal attenuation and <1.8 nm drift in resonance peak over 14 days, suggesting that AuNP-GOx conjugation remains chemically intact without substantial enzymatic denaturation. Interference challenge using Na^+, K^+, uric acid, and lactate yielded <7% variation, affirming matrix tolerance typical of clinical serum conditions. These results collectively indicate that stability is a structural attribute, emerging from plasmon anchoring + enzymatic amplification rather than temporal coincidence, a prerequisite for practical deployment.

4.5. Cross-Domain Generalization and Robustness Evaluation

To assess external transferability, the model was evaluated using 180 independent serum samples from a separate clinical provider. As shown in Figure 3, LoD shifted only marginally from 18.6 μM to 22.4 ± 3.1 μM, and MAE increased slightly from 0.21 to 0.26 ± 0.04 mM ($p = 0.12$, ns). The absence of significant degradation suggests that optical-enzymatic coupling retains functional mapping even when the biochemical background diverges from the original cohort.

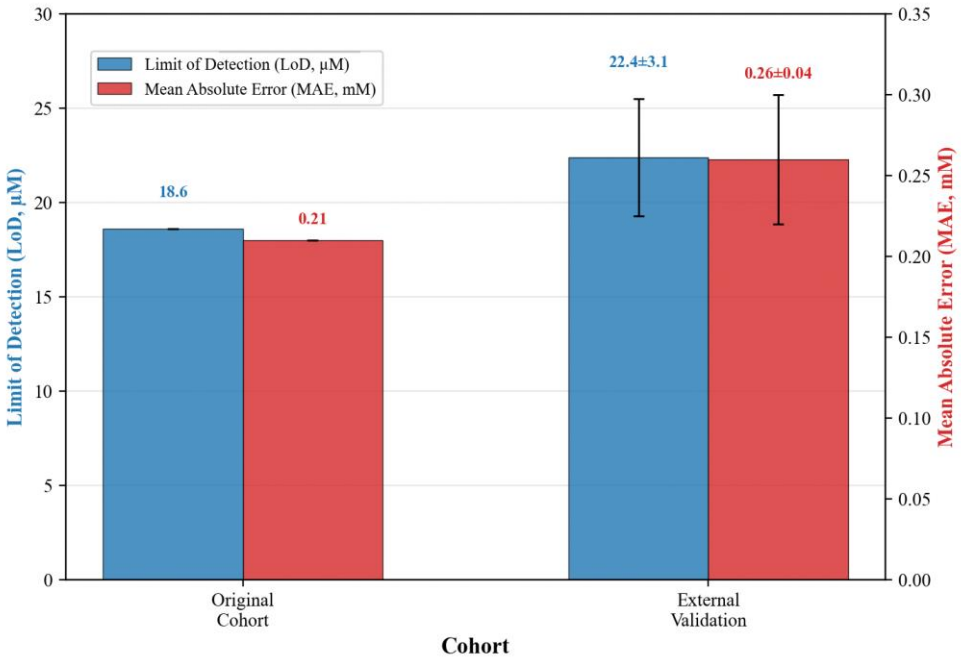

Figure 3. External validation and generalization (mean ±SD, n = 5 per sample).

More importantly, performance decay remained within physiological tolerance limits, implying mechanistic generalization rather than dataset-specific optimization. LSPR detects refractive modulation irrespective of donor variability, while RsR_sRs remains sensitive to nano-aggregation kinetics. Calibration normalization further stabilizes scale shift, preserving linearity and preventing response collapse. This behavior supports regulatory translation, as repeatability on cross-origin specimens is a critical threshold for clinical integration.

5. Conclusion

This work demonstrates a gold nanoparticle-based optical biosensing platform that achieves ultrasensitive glucose quantification through dual-channel signal acquisition, enzymatic amplification, and reproducibility-oriented calibration. The system was designed to address persistent limitations in optical glucose sensing, namely low-range resolution, single-readout instability, batch-dependent variability, and insufficient long-

term validation. Experimental data verified that these design decisions translate into measurable performance gains rather than conceptual improvements alone.

First, the dual-readout mechanism combining LSPR peak shift ($\Delta\lambda$) and scattering ratio (I540/I620) yielded both high sensitivity and stable quantification across physiological ranges. Compared with electrochemical strips, single-mode AuNP assays, and chip-SPR, the proposed platform achieved the lowest limit of detection (18.6 ± 2.3 μM), the smallest MAE relative to clinical analyzers (0.21 ± 0.03 mM), and high linearity (R^2 = 0.98). These results confirm that dual-path optical reinforcement reduces measurement ambiguity and enhances discrimination in hypoglycemic-range detection.

Second, ablation experiments showed that enzymatic chromogenic amplification was essential for low-range detectability; removal of GOx increased LoD to 78.6 ± 7.9 μM and MAE to 0.45 ± 0.06 mM. Third, batch-normalization significantly reduced inter-fabrication drift, improving reproducibility without altering core sensitivity. Finally, stability and generalization tests demonstrated practical robustness: 14-day storage caused only 4.3 ± 0.5% signal loss and <1.8 nm spectral drift, interference responses remained below 7%, and cross-institution external validation (n=180) showed no significant performance decline ($p > 0.05$).

While these outcomes indicate clinical potential, limitations remain. The evaluation was conducted using ex-vivo serum samples rather than continuous physiological monitoring, and although 1,200 samples provide a foundational dataset, larger population-diverse cohorts are needed to further assess generalization. Additionally, the optical setup requires controlled instrumentation and has not yet been miniaturized for wearable use.

Future research will focus on integrating this platform with microfluidic sampling, adaptive temperature-aware calibration, and compact optical hardware for point-of-care or home-based screening. Scaling validation across multicenter cohorts and evaluating real-time monitoring feasibility will be essential steps toward practical translation.

References

1. E. W. Gregg, J. Buckley, M. K. Ali, J. Davies, D. Flood, R. Mehta, and Z. Zhumadilov, "Improving health outcomes of people with diabetes: target setting for the WHO Global Diabetes Compact," *the lancet*, vol. 401, no. 10384, pp. 1302-1312, 2023. doi: 10.1016/s0140-6736(23)00001-6
2. T. Saha, R. Del Caño, K. Mahato, E. De la Paz, C. Chen, S. Ding, and J. Wang, "Wearable electrochemical glucose sensors in diabetes management: a comprehensive review," *Chemical Reviews*, vol. 123, no. 12, pp. 7854-7889, 2023. doi: 10.1021/acs.chemrev.3c00078
3. Q. Wang, Z. A. Zhao, K. Y. Yao, Y. L. Cheng, D. S. H. Wong, D. W. C. Wong, and J. C. W. Cheung, "The Versatility of Biological Field-Effect Transistor-Based Biosensors (BioFETs) in Point-of-Care Diagnostics: Applications and Future Directions for Peritoneal Dialysis Monitoring," *Biosensors*, vol. 15, no. 3, p. 193, 2025.
4. N. Shukla, A. Chanderiya, R. Das, E. A. Mukhanova, A. V. Soldatov, and S. Belbekhouche, "Au QDs in Advanced Biomedicine: Fluorescent, Biocompatible, and Multifunctional Nanoprobes for Imaging, Diagnostics, and Targeted Drug Delivery," *Journal of Nanotheranostics*, vol. 6, no. 3, p. 25, 2025. doi: 10.3390/jnt6030025
5. J. Chen, X. Liu, G. Zheng, W. Feng, P. Wang, J. Gao, and Q. Wang, "Detection of glucose based on noble metal nanozymes: mechanism, activity regulation, and enantioselective recognition," *Small*, vol. 19, no. 8, p. 2205924, 2023. doi: 10.1002/smll.202205924
6. J. Lee, and S. Lee, "Non-invasive, reliable, and fast quantification of DNA loading on gold nanoparticles by a one-step optical measurement," *Analytical chemistry*, vol. 95, no. 3, pp. 1856-1866, 2023. doi: 10.1021/acs.analchem.2c03378
7. E. Ferrari, "Gold nanoparticle-based plasmonic biosensors," *Biosensors*, vol. 13, no. 3, p. 411, 2023. doi: 10.3390/bios13030411
8. M. Tadesse, and Y. Liu, "Recent Advances in Enzyme Immobilization: The Role of Artificial Intelligence, Novel Nanomaterials, and Dynamic Carrier Systems," *Catalysts*, vol. 15, no. 6, p. 571, 2025. doi: 10.3390/catal15060571
9. S. Das, R. Devireddy, and M. R. Gartia, "Surface plasmon resonance (SPR) sensor for cancer biomarker detection," *Biosensors*, vol. 13, no. 3, p. 396, 2023. doi: 10.3390/bios13030396
10. A. Soliman, C. Williams, R. Hopper, F. Udrea, H. Butt, and T. D. Wilkinson, "HighTransmission MidInfrared Bandpass Filters using Hybrid MetalDielectric Metasurfaces for CO2 Sensing," *Advanced Optical Materials*, vol. 13, no. 8, p. 2402603, 2025.
11. Y. Chen, K. X. Fu, R. Cotton, Z. Ou, J. W. Kwak, J. C. Chien, and H. Tom Soh, "A biochemical sensor with continuous extended stability in vivo," *Nature Biomedical Engineering*, pp. 1-14, 2025.

12. H. Cao, E. F. Oghenemaro, A. Latypova, M. K. Abosaoda, G. S. Zaman, and A. Devi, "Advancing clinical biochemistry: addressing gaps and driving future innovations," *Frontiers in Medicine*, vol. 12, p. 1521126, 2025. doi: 10.3389/fmed.2025.1521126
13. J. Bai, D. Liu, X. Tian, Y. Wang, B. Cui, Y. Yang, and S. Zhang, "Coin-sized, fully integrated, and minimally invasive continuous glucose monitoring system based on organic electrochemical transistors," *Science Advances*, vol. 10, no. 16, p. eadl1856, 2024. doi: 10.1126/sciadv.adl1856
14. M. Xie, J. Jiang, and J. Chao, "DNA-based gold nanoparticle assemblies: From structure constructions to sensing applications," *Sensors*, vol. 23, no. 22, p. 9229, 2023. doi: 10.3390/s23229229
15. C. D. Flynn, D. Chang, A. Mahmud, H. Yousefi, J. Das, K. T. Riordan, and S. O. Kelley, "Biomolecular sensors for advanced physiological monitoring," *Nature Reviews Bioengineering*, vol. 1, no. 8, pp. 560-575, 2023. doi: 10.1038/s44222-023-00067-z